Modeling, control, and power management for a grid-integrated photo voltaic, fuel cell, and wind hybrid system

Ezhilarasan GANESAN*, Subhranhsu Sekhar DASH, Chinmaya SAMANTA
Department of Electrical and Electronics Engineering, SRM University, Kancheepuram, India

Abstract: Power management in a grid-integrated power system consisting of distributed renewable energy sources is necessitated by ever-increasing energy consumption, the high cost of production, the limited resource of fossil fuel, and the worsening global environment. Wind and solar power generation are two of the most promising renewable power generation technologies. The growth of wind and photovoltaic (PV) power generation systems has exceeded the most optimistic levels of expectations. Fuel cells (FCs) also have great potential to be green power sources of the future because of the many merits they have, such as high efficiency and zero or low emission of pollutant gases. In this paper the modeling, control, and analysis of grid-connected PV power, a proton exchange membrane fuel cell (PEMFC), and a wind energy system (WES) connected through a common DC bus linked to an AC grid is discussed. In coordination with the PEMFC, the hybrid system's output power becomes controllable so that full utilization of PV and wind power takes place based on its availability, and the DC bus voltage is maintained constant even at varying load conditions for the desired power sharing between the distributed generation (DG) sources, load, and the AC grid. The hybrid system is controlled through a combination of two proposed control modes, namely the DG control mode and grid control mode. The coordination of the power controller, voltage source converter controller, and load controller is such that the transition between the two control modes is done as smoothly as possible. Thus, the total DG power will be a combination of PV power, WES power, and power produced by the PEMFC. Any additional power if required up to the maximum loading will be supplied by grid. If the load exceeds its maximum value, then the load controller will carry out load shedding. The composite system is available for safe operation in on-grid as well as off-grid mode satisfying voltage and power balance constraints. Different modes of operation have been demonstrated to verify and validate the desired power management among the DG sources, load, and the grid. MATLAB/Simulink software was used for simulating the composite model.

Key words: Distributed generation, grid-controlled mode, distributed generation control mode, wind energy system, power management, fuel cell

1. Introduction

A major percentage of all electrical power is produced through conventional energy sources alone; hence, the reserves of coal and fossil fuels are diminishing at a fast rate. Therefore, due to these limitations, a new method has to be found to balance supply and demand without resorting to conventional generation, as stated in [1]. Initially, alternate sources of energy like solar and wind power sources were installed with the primitive equipment available, which resulted only in generation of additional energy without proper management of

---
*Correspondence: ezhil.power@gmail.com

generated power. Over recent years several research and investment programs have been carried out with hybrid power systems, which recommend an optimal design model for hybrid solar–wind systems [2]. Recently, electronic power converters and their identified usage for power systems have brought about many changes, like the concept of distributed generation using hybrid power generation. The importance of hybrid systems consisting of renewable energy (RE) sources has increased significantly as they appear to be an effective solution for clean and distributed energy production. This consists of renewable energy sources such as photovoltaic (PV) energy, wind generators, and fuel cells (FCs) along with the necessary power converters.

At present, distributed generation is assuming increased importance because of its several distinctive advantages, such as simple configuration, multiple sources, high reliability, absence of fuel costs, low maintenance, and the fact it has absolutely no pollutants and hence is ecofriendly.

Many alternative energy sources including wind, PV, FCs, diesel systems, gas turbines, and microturbines can be used to build hybrid energy systems. Nevertheless, the major renewable energy sources used and reported are wind and PV power, as stated in [3]. However, the disadvantage of PV generation and wind energy systems (WESs) is that they are characteristically unstable, being heavily dependent on weather conditions. Stand-alone wind and PV energy systems normally require energy storage devices. The storage device can be an electrochemical battery, ultracapacitor, magnetic energy storage, and so on.

In order to overcome the inherent drawbacks discussed above, distributed generation (DG) sources such as PV and WESs should be combined with a proton exchange membrane fuel cell (PEMFC) to form a hybrid system. By changing the FC output power, the hybrid source output becomes controllable and can be maintained at a certain reference level. However, a PEMFC in turn works only at high efficiency within a specific power range. This proposed hybrid system can be linked to the main grid or can work independently, and when in grid-connected mode the hybrid source is connected to the main grid at the point of common coupling (PCC) to deliver power to the load. Whenever the demand from the load changes, the power supplied by the main grid and hybrid system must be properly managed. The power delivered from the main grid and the PV array, as well as the PEMFC, must be coordinated to meet load demand. The hybrid generation thus can be controlled in 2 control modes: grid control mode (GCM) and distributed generation control mode (DGCM), as stated in [4]. In GCM mode, variations of load demand are compensated by the main grid because the hybrid source output is regulated by the reference power. The proposed operating strategy is to coordinate the two control modes and determine the reference values of the DGCM mode so that all constraints are satisfied. This operating strategy will minimize the number of operating mode changes, improve the performance of the system operation, and enhance system stability.

2. Working methodology of a grid-integrated hybrid system

This paper presents modeling and control strategies for power and load management of a grid-integrated hybrid system consisting of a PV array, a PEMFC, and a WES connected through a common DC link to an AC grid as stated in [5].

The coordination of the power controller, voltage source converter (VSC) controller, and load controller is proposed to make the transition between the two modes as smooth as possible. The load is connected between the DG sources and grid. With the varying load conditions, the DG output power (Pms) and grid power (Pgrid) must be properly adjusted and coordinated so as to match the load (Pload), while fully utilizing the PV power and WES to keep the DC bus voltage constant.

The grid-integrated hybrid system mainly works in 2 modes of operation: DGCM and GCM. As stated

earlier, the power controller referred to in [6] coordinates the automatic change-over between these two modes in coordination with the load controller and the inverter controller.

The system operates in DGCM when the load is less than a certain threshold (P_{thload}) value. The output power of the DGs is maintained at a certain reference level (P_{msref}) based on PV power availability by varying the FC power with proper coordination [7]. When the power drawn by the load is greater than or equal to the threshold value, but less than the maximum load ($P_{loadmax}$), the hybrid system will be in GCM. FCs will deliver fixed power operating at the lowest level (P_{fclow}).

In order to achieve a reliable DG setup with reduced grid dependency, the various modules of the DG were mathematically modeled and integrated as follows: modeling of wind turbine, drive train, maximum power point tracker (MPPT), pitch angle controller, permanent-magnetic synchronous generator (PMSG), DC/DC converter, and the power controllers. After the modeling, the integration of a PV-FC-wind hybrid system to the grid was done followed by the implementation of controlled mode (auto) and noncontrolled (manual) mode of operation. Thus, the full utilization of PV and wind power was possible by maintaining a constant DC bus voltage to achieve the desired power management between DG sources, load, and grid under all load conditions. In the case of the power being unmanageable, local power shedding is used.

3. Modules of the grid-integrated hybrid system

The grid-integrated hybrid system, as shown in Figure 1, consists of 3 nonconventional energy sources, namely a solar photovoltaic arrangement with a DC-DC boost converter with a perturb and observe MPPT algorithm, a proton exchange membrane-based fuel cell with DC boost converter, and a wind energy system with its output suitably rectified and stepped up in order to match the voltage of the common DC bus of the DG system. Thus, P_{pv}, P_{wind}, and P_{fc} are obtained at the same DC level.

In order to connect DG sources to the load and the grid, the output from the DG sources is given to a DC bus, which is further connected to a DC to 3 phase inverter VSC, from where the power P_{ms} is fed to a 3-phase transformer and hence to the load and grid. The power fed to the grid is marked as P_{grid} and that to that of the load is marked P_{load}. In the next section the details of the modeling of the above-mentioned modules of the grid-integrated hybrid power system are discussed.

3.1. Modeling of photovoltaic arrays

The mathematical equations that describe the voltage-current (V-I) characteristic of the ideal photovoltaic cell as referred to in [8] are:

$$I = I_{pvcell} - I_d \text{ and } I_d = I_{ocell}[\exp(qV/akT) - 1], \tag{1}$$

where I_{pvcell} is the current generated by the incident light, which is directly proportional to the solar irradiation; I_d is the Shockley diode equation; I_{0cell} is the reverse saturation or leakage current of the diode; q is the electron charge ($1.60217646 \times 10^{-19}$ C); k is the Boltzmann constant ($1.3806503 \times 10^{-23}$ J/K); K is the working temperature of the p-n junction; and a is the diode ideality factor as referred to in [9].

$$I = I_{pv} - I_o[\exp[(V + R_sI)/(aV_t)] - 1], \tag{2}$$

where I_{pv} and I_0 are the photovoltaic and saturation currents of the array and $V_t = (N_skT)/q$ is the thermal voltage of the array with N_s cells in series. R_s and R_p are the equivalent series and parallel resistance of the
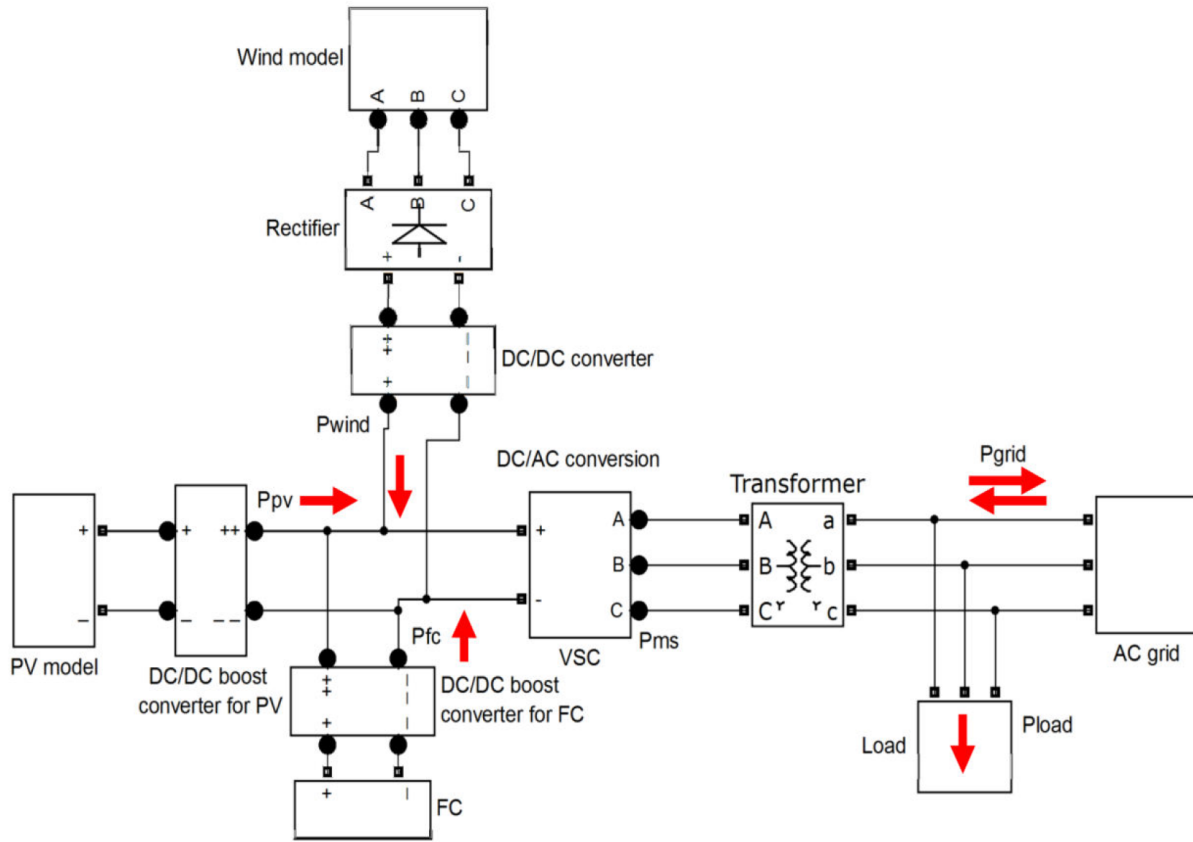
Figure 1. Overall arrangement of grid-integrated hybrid power generation.

array as referred to in [10].

$$I_{pv} = (I_{pvn} + K_I \Delta T) \times (G/G_n), \tag{3}$$

where I_{pvn} is the light-generated current at the nominal condition (usually 25 °C and 1000 W/m^2), $\Delta T = T$ – T_n (T and T_n are the actual and nominal temperatures K), G [W/m^2] and G_n [W/m^2] are the operating and nominal irradiation, and K_I is the current/temperature coefficient in A/K. The diode saturation current I_0 depends on temperature, as given by;

$$I_0 = (I_{scn} + K_I \Delta T)/[\exp\{V_{ocn} + K_V \Delta T)/(aV_t)\} - 1], \tag{4}$$

where I_{scn} is the nominal short-circuit current, V_{ocn} is the nominal open-circuit voltage, and K_V is the voltage/temperature coefficient in V/K. If the photovoltaic array is composed of N_{ser} series and N_{par} parallel modules, then

$$I = I_{pv} + N_{par} - I_o N_{par}[\exp\{\{V + R_s(N_{ser}/N_{par})I\}\Delta T)/(aV_t N_{ser})\} - 1]. \tag{5}$$

The PV array maximum power output is given by

$$P_{MPP} = V_{MPP} \times I_{MPP}. \tag{6}$$

3.2. Maximum power point tracker control

The role of the MPPT in PV systems is to automatically track the voltage V_{MPP} or current I_{MPP} at which a PV array should operate to obtain the maximum power output P_{MPP} under a given operating temperature and irradiance. Most MPPT techniques respond to changes in both irradiance and temperature. In the present work, the incremental conductance (INC) method is used, in which the problem of tracking peak power under fast varying atmospheric condition is resolved. The INC method, as referred to in [11], is based on the fact that the slope of the PV array power is zero at the MPP, positive on the left of the MPP, and negative on the right, as shown in Figure 2.
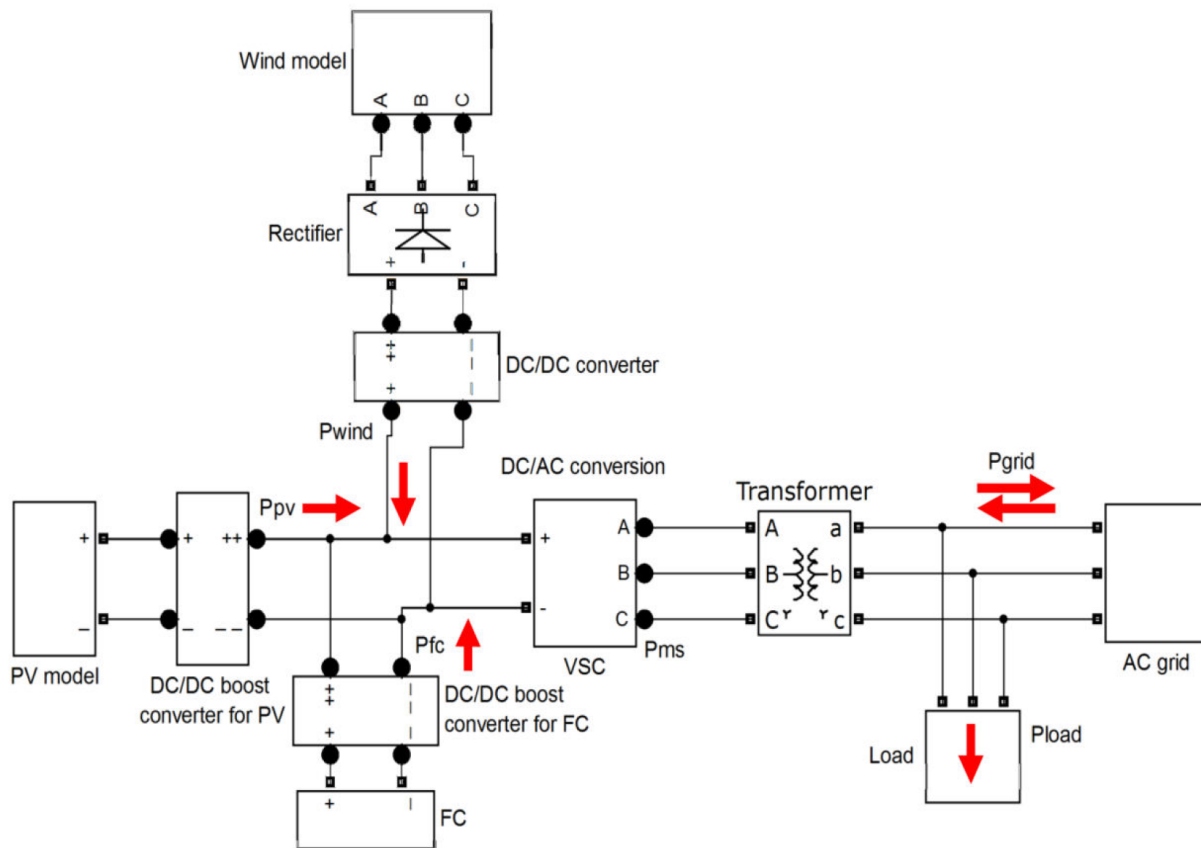

Figure 2. Incremental conductance algorithm P-V/P-I characteristic.

Therefore, $\Delta I/\Delta V = -I/V$ at the MPP, $\Delta I/\Delta V > -I/V$ on the left of the MPP, and $\Delta I/\Delta V < -I/V$ on the right of the MPP. The MPP can thus be tracked by comparing the instantaneous conductance (I/V) with the incremental conductance $(\Delta I/\Delta V)$ as stated in [12].

3.3. Modelling of the fuel cell

The PEMFC, as shown in Figure 3, is a nonlinear, multiple-input and multiple-output, strongly coupled, and large-delay dynamic system that converts chemical potential into electric power. It converts the chemical energy of a fuel.
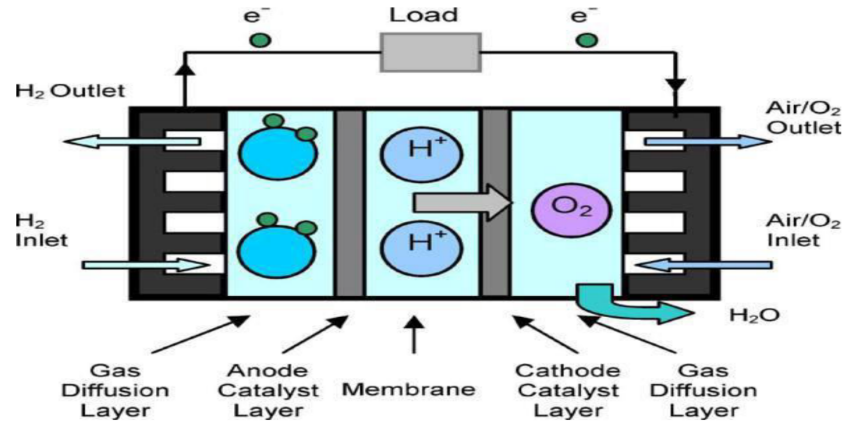
Figure 3. Proton exchange membrane fuel cell.

The electrochemical model of a fuel cell is based upon mathematical equations as referred to in [13]. The output voltage of a FC can be defined as:

$$V_{fc} = E_{nerst} - V_{act} - V_{ohm} - V_{copc}, \qquad (7)$$

where Vfc = fuel cell voltage, E_{nerst} = reversible or open-circuit voltage, V_{act} = actual voltage or activation potential between anode and cathode, V_{ohm} = ohmic voltage drop, and V_{conc} = concentration voltage or voltage drop due to exchange of charged carriers.

$$E_{nerst} = \zeta_1 - \zeta_2 * (T_{fc} - T_{nfc}) + \zeta_3 * T * [\ln(PH_2) + 0.5 * \ln(PO_2)], \qquad (8)$$

where ζ_1 through ζ_4 are constants and T and T_{fc} are operating temperatures in K, T_{nfc} is the reference temperature in K, PH_2 is the partial pressure of hydrogen in N/m^2, and PO_2 is the partial pressure of the oxygen in N/m^2. The activation potential between anode and cathode is given by:

$$V_{act} = -[\zeta_1 + \zeta_2 * T_{fc} + \zeta_3 * T_{fc} * \ln(CO_2) + \zeta_4 * \ln(I_{stack})], \qquad (9)$$

where I_{stack} is the operating current of the fuel cell, ζ_1 through ζ_4 are parametric coefficients of FC, and $CO_2 = PO_2 / \left[C_1 \times 10^2 \times e^{\frac{C2}{T}} \right]$ with C_1 and C_2 being constants. The ohmic drop is given by:

$$V_{ohm} = I_{stack} * (R_m + R_c), \qquad (10)$$

where R_c is the resistance to the transfer of protons through the membrane. R_m is the resistance of the membrane to the electron flow. The voltage drop is given by:

$$V_{conc} = -\beta_k * \left[\ln\left(1 - \left(\frac{J}{J_{\max}} \right) \right) \right], \qquad (11)$$

where β is a parametric coefficient of the fuel cell, and J and J_{max} are the actual and maximum current densities of the cell. The simulation model of the FC is shown in Figure 4. Figure 5 shows the MATLAB simulation model of the boost converter used for the fuel cell. Figure 6 shows the output voltage of the fuel cell.
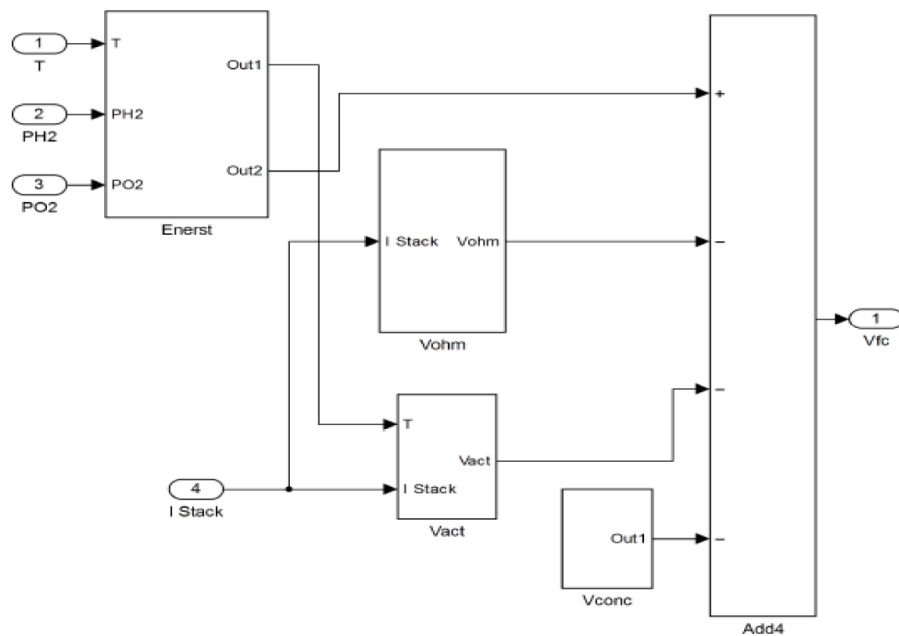
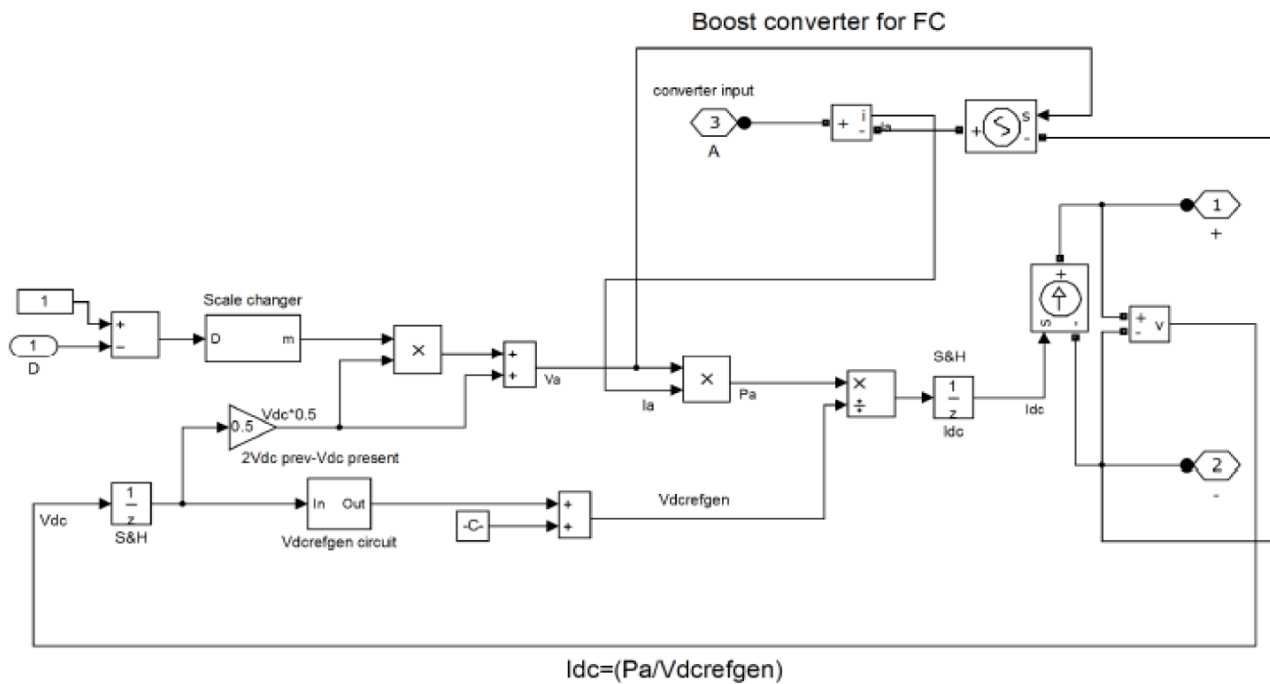**Figure 4.** MATLAB simulation model of fuel cell.

Figure 5. MATLAB simulation model of boost converter used for fuel cell.

3.4. Wind energy system mathematical model and simulation

The WES as shown in Figure 7 mainly consists of a variable-speed wind turbine with a drive train (to drive the rotor shaft), pitch angle controller, PMSG, rectifier, MPPT, DC/DC converter, and DC/AC converter, as
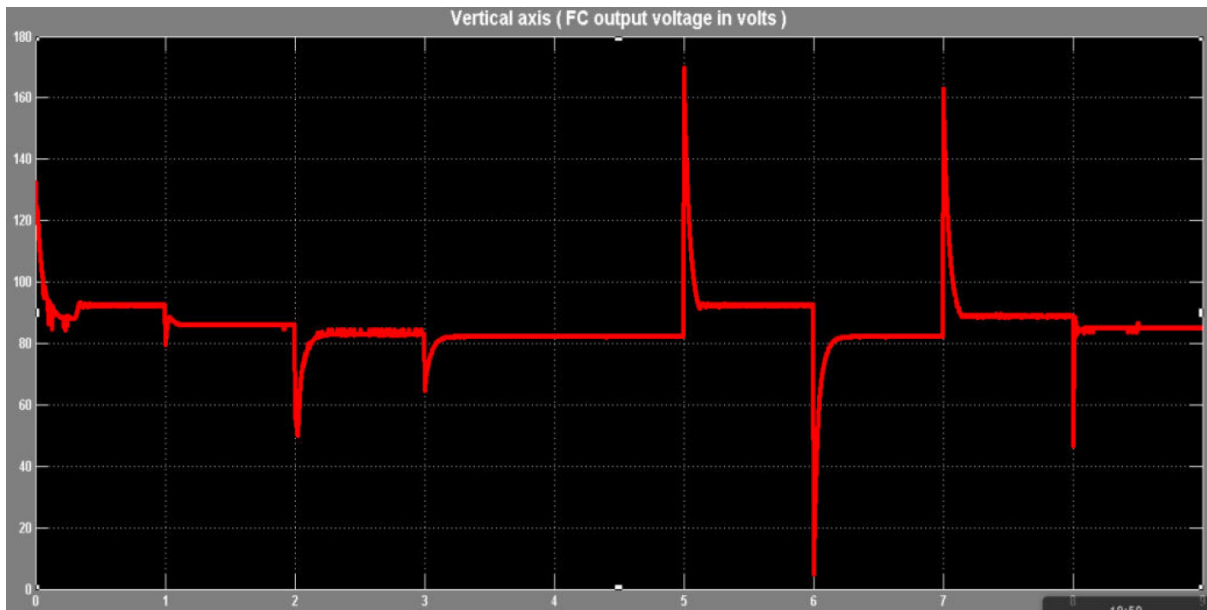
Figure 6. Output voltage of a fuel cell.

referred to in [14]. The pitch angle controller takes care of the pitch of the WES such that in the case of high wind speed or low wind speed the pitch can be adjusted as referred to in [15] to operate the wind turbine at its optimum level. A permanent magnet synchronous generator is preferred because of its simple construction and low maintenance. The mathematical model of the WES was derived by removing the wind energy system from the grid-integrated hybrid system. Thus, as per the model, the WES supplies the grid, and hence the load, directly. This is done in order to study the individual behavior of the WES so that when it is integrated into the hybrid system the control parameters can be easily set and an accurate control can be achieved. The output power of the turbine was referred to in [16] and is given by the following equations.
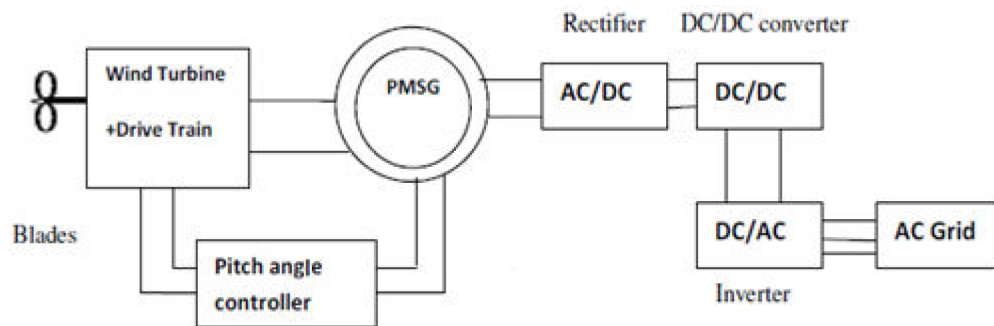

Figure 7. Schematic of a wind energy system.

$$P_m = C_p \times (\omega_\omega)^3 \tag{12}$$

$$T_t = \frac{P_m}{\omega_{sh}} \tag{13}$$

$$\lambda = \left(\frac{\omega_{sh}}{\omega_\omega} \right) * \lambda_{nom} \tag{14}$$

$$C_p = C_1 + \left[\frac{C_2}{\lambda - C_3} * \beta - C_4 \right] * \exp\left(\frac{-C_5}{\lambda} \right) + C_6 * \lambda \tag{15}$$

$$\frac{1}{\lambda_i} = \frac{1}{[\lambda + 0.08 * \beta]} - \frac{0.0.35}{\left[(\beta)^3 + 1\right]} \tag{16}$$

$$C_{pnom} = C_{p\,\max} \tag{17}$$

$$\lambda_{inom} = \left(\frac{1}{\frac{1}{\lambda_{nom}} - 0.035} \right) \tag{18}$$

$$K_{nom} = - \frac{\left(C_2 * \frac{C_5}{\lambda_{inom}} - C_4 * C_5 - C_2 \right) * \exp\left(\frac{-C_5}{\lambda_{inom}} \right)}{(\lambda_{nom})^2} \tag{19}$$

$$C_1 = \frac{C_{p\,\max}}{\left(\left(\frac{C_2}{\lambda_{inom}} - C_4 \right) * \exp\left(\frac{-C_5}{\lambda_{inom}} \right) + K_{nom} * \lambda_{nom} \right)} \tag{20}$$

$$C_6 = K_{nom} * C_1 \tag{21}$$

Here, P_m is the mechanical output power of the turbine, C_p is the performance coefficient of the wind turbine, ω_ω is the wind speed in m/s, T_t is the output torque of the turbine, ω_{sh} is the shaft speed in m/s, λ is the tip speed ratio of the rotor blade tip speed to wind speed, λ_i is the initial value of λ, λ_{nom} is the rated value of λ, C_1 to C_6 are turbine constants, β is the blade pitch angle in degrees, C_{pnom} is the rated value of C_p, and C_{pmax} is the maximum value of C_p.

3.4.1. Drive train model

The drive train as modeled in Figure 8 is the connection between the wind turbine and the synchronous generator, which drives the shaft connecting them. The shaft torque gains importance because it generates the equivalent AC voltage from the WES. The shaft torque in this work was maintained at an optimum level, even for high wind impact on the turbine, by simply adjusting the pitch angle. Hence, in modeling the drive train the turbine torque T_t was set at a per unit quantity that resulted in shaft torque T_{sh} as per Eq. (13). It can be noted from Eq. (11) that not all the turbine torque gets converted into T_m. The per unit T_{sh} was converted to T_m, the output mechanical torque, by multiplying the shaft torque by T_{base} as shown in Eq. (15). The modeling of the drive train is hence given by the following mathematical equations.
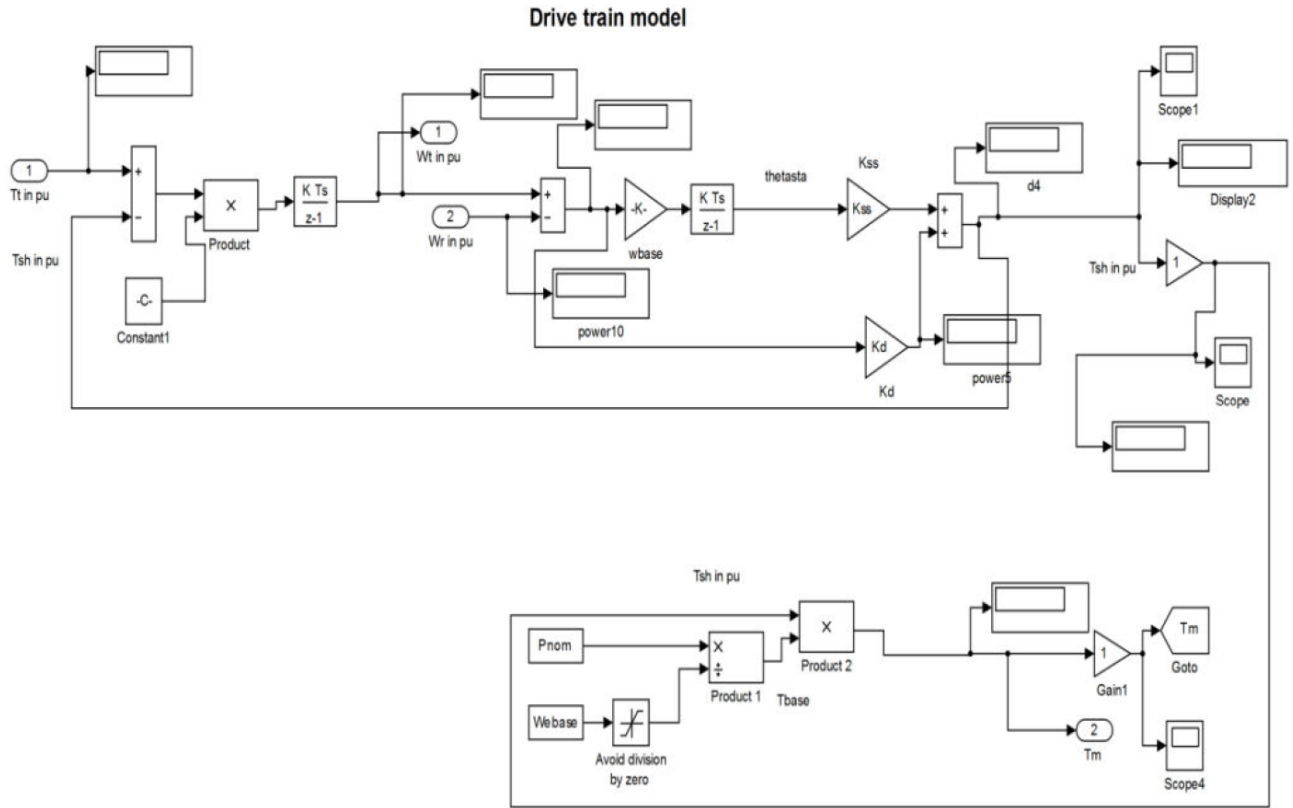
Figure 8. MATLAB model of the drive train.

$$T_t - T_{sh} = 2 * H_t * \left(\frac{d\omega_t}{dt} \right) \tag{22}$$

$$\frac{(\omega_t - \omega_r)}{\omega_{ebase}} = \left[\frac{d(\theta_{sta})}{dt} \right] \tag{23}$$

$$T_{sh} = [\theta_{sta} * K_{ss} + K_d * (\omega_{t-}\omega_r)] \tag{24}$$

$$T_{base} = \frac{P_{nom}}{\omega_{ebase}} \tag{25}$$

$$T_m = T_{base} + T_{sh} \tag{26}$$

Here, H_t is the inertia constant of the turbine, ω_t is the angular speed of the wind turbine, ω_r is the rotor speed of generator, θ_{sta} is the shaft twist angle, K_{ss} is the shaft stiffness coefficient, K_d is the damping coefficient, ω_{ebase} is the electrical base speed, P_{nom} is the nominal power of WES, and T_{base} is the base torque of the wind turbine. The above parameters are depicted in Figure 9.
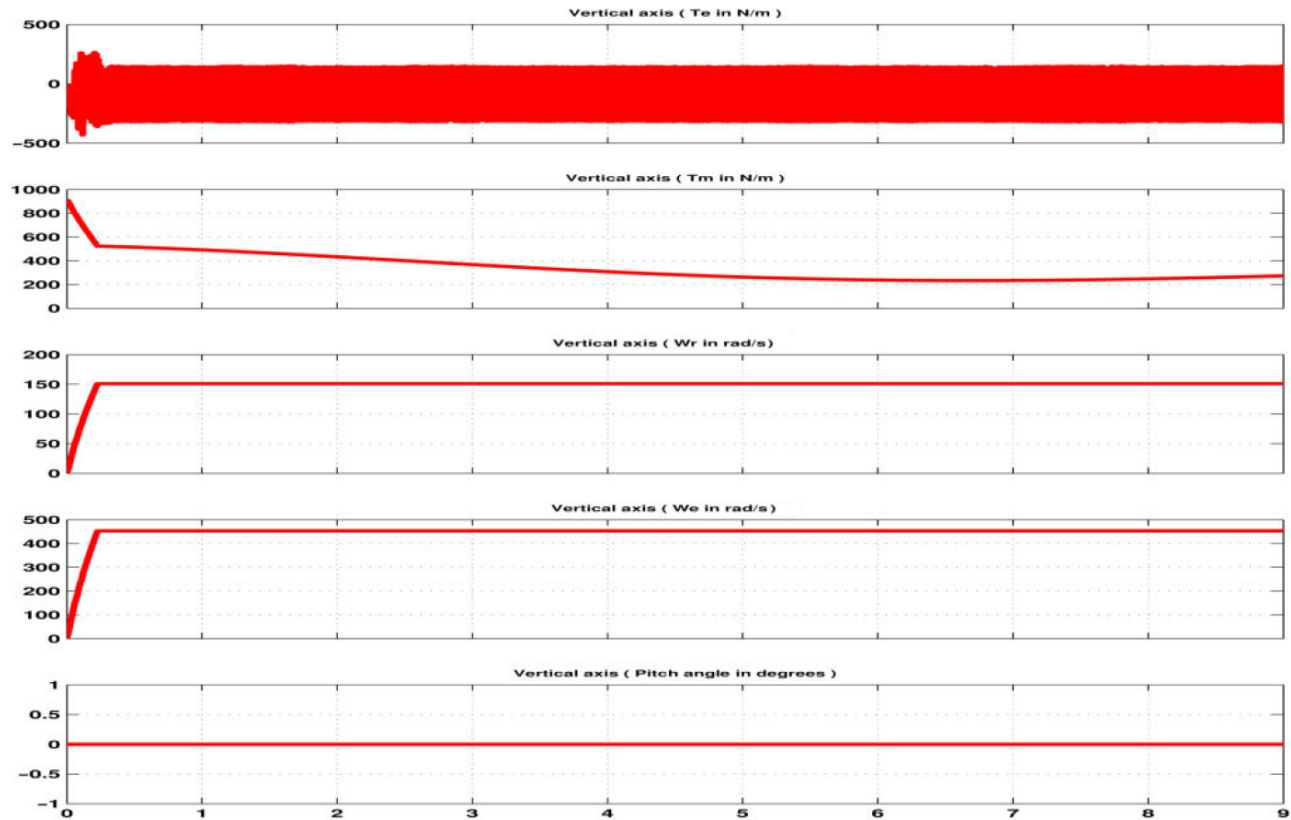
Figure 9. Various output parameters of wind energy system.

4. Permanent magnet synchronous generator modeling

The permanent magnet synchronous generator is where the excitation field is provided by a permanent magnet instead of a coil. Synchronous generators are the main source of commercial electrical energy. They are commonly used to convert the mechanical power output of wind turbines into electrical power for the grid.

A set of 3 conductors make up the armature winding. The phases are wound such that they are 120° apart spatially on the stator, providing for a uniform force or torque on the generator rotor. The uniformity of the torque arises because the magnetic fields resulting from the induced currents in the 3 conductors of the armature winding combine spatially in such a way as to resemble the magnetic field of a single rotating magnet. This stator magnetic field or "stator field" appears as a steady rotating field and spins at the same frequency as the rotor when the rotor contains a single dipole magnetic field. The two fields move in "synchronicity" and maintain a fixed position relative to each other as they spin.

The advantage of using permanent magnet generators in this work is that they do not require a DC supply for the excitation circuit, nor do they have slip rings and contact brushes, and hence the maintenance is simple. The drawback of the PMSG is that the flux density of high-performance permanent magnets is limited. The air gap flux is also not controllable, so the voltage of the machine cannot be easily regulated. Hence, here in this modeling all the above factors are considered and suitably modeled.

The modeling of PMSG was referred to in [17] and is carried out using the following mathematical

equations.

$$\left(d\frac{I_d}{dt}\right) = \left(\frac{V_d}{L_d}\right) + \omega_e * I_q * \left(\frac{L_q}{L_d}\right) - I_d * \left(\frac{R}{L_d}\right) \tag{27}$$

$$\left(d\frac{I_q}{dt}\right) = \left(\frac{V_q}{L_q}\right) - \omega_e * I_d * \left(\frac{L_d}{L_q}\right) - \omega_e * \left(\frac{\lambda_o}{L_q}\right) - I_q * \left(\frac{R}{L_q}\right) \tag{28}$$

$$T_e = \left(\frac{3}{2}\right) * P\left(\lambda_o * I_q + (L_d - L_q) * I_d * I_q\right) \tag{29}$$

$$\left(d\frac{\omega_r}{dt}\right) = \frac{(T_m - T_e - F * \omega_r)}{J} \tag{30}$$

$$P * \omega_r = \omega_e \text{ and } \left(d\frac{\theta}{dt}\right) = \omega_e \tag{31}$$

$$I_a = I_d * \sin\theta + I_q * \cos\theta + I_o \tag{32}$$

$$I_b = I_d * \sin\left[\theta - \left(\frac{2\pi}{3}\right)\right] + I_q * \cos\left[\theta - \left(\frac{2\pi}{3}\right)\right] + I_o \tag{33}$$

$$I_c = I_a - I_b \tag{34}$$

I_a and I_{br} will have the same expressions while I_{cr} will be:

$$I_{cr} = I_d * \sin\left[\theta + \left(\frac{2\pi}{3}\right)\right] + I_q * \cos\left[\theta + \left(\frac{2\pi}{3}\right)\right] + I_o, \tag{35}$$

$$V_q = \left(\frac{1}{3}\right) * (2V_{ab} + V_{bc}) * \cos\left[\theta + \left(\frac{1}{\sqrt{3}}\right)\right] * V_{bc} * \sin\theta, \tag{36}$$

$$V_q = \left(\frac{1}{3}\right) * (2V_{ab} + V_{bc}) * \cos\left[\theta + \left(\frac{1}{\sqrt{3}}\right)\right] * V_{bc} * \sin\theta, \tag{37}$$

where R is the stator winding resistance in ohm, L_d is the d-axis inductance in henry, L_q is the q-axis inductance in henry, I_q is the q-axis current, I_d is the d-axis current, V_q is the q-axis voltage, V_d is the d-axis voltage, ω_r is the angular velocity of the rotor in rad/s, λ_o is the amplitude of flux induced in Wb, P is the number of pole pairs, ω_e is the angular electrical speed in rad/s, J is the rotor inertia, F is the rotor friction, θ is the rotor angle, and I_a, I_b, and I_c are the stator phase currents.

4.1. Permanent magnet synchronous generator controller

The output of the PMSG from the MATLAB simulation circuit is shown in Figure 10. The controller circuit of the PMSG is shown in Figure 11. It can be seen that the stator currents are compared with the reference values in the comparator to obtain a control voltage of Vab and Vbc as in [18]. Figure 12 shows the simulation model of the wind energy system with rectifier DC-DC converter and MPPT.
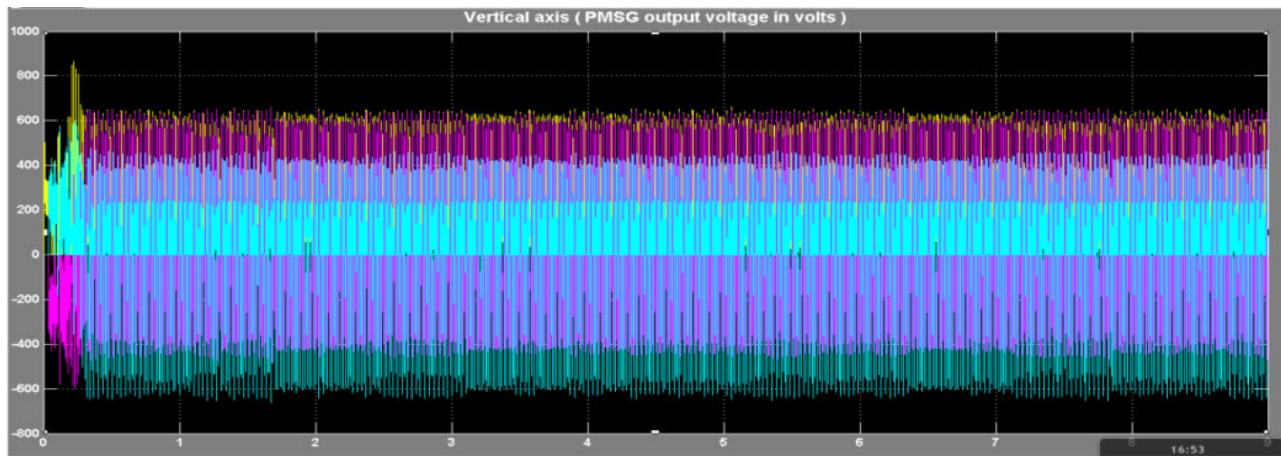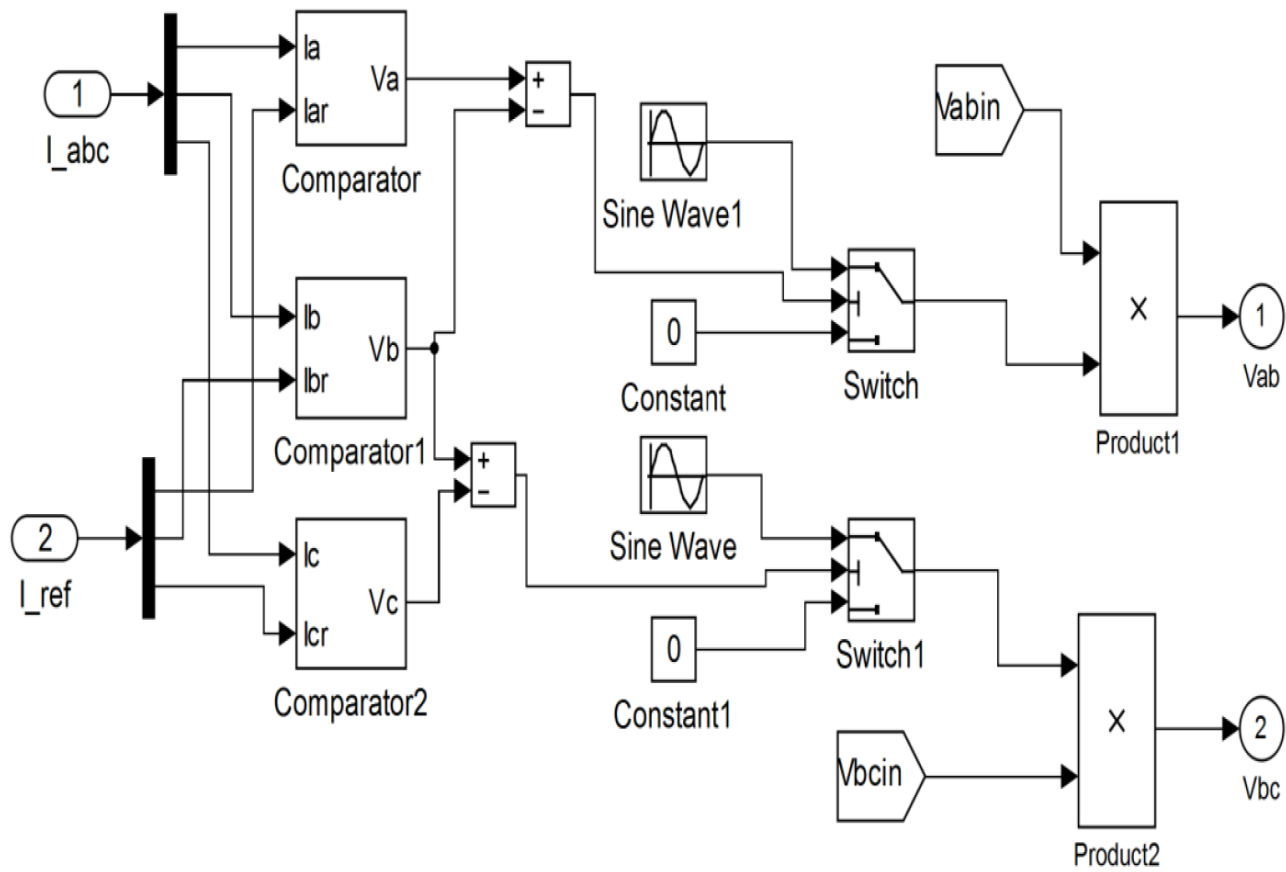
Figure 10. Three phase PMSG output voltage.

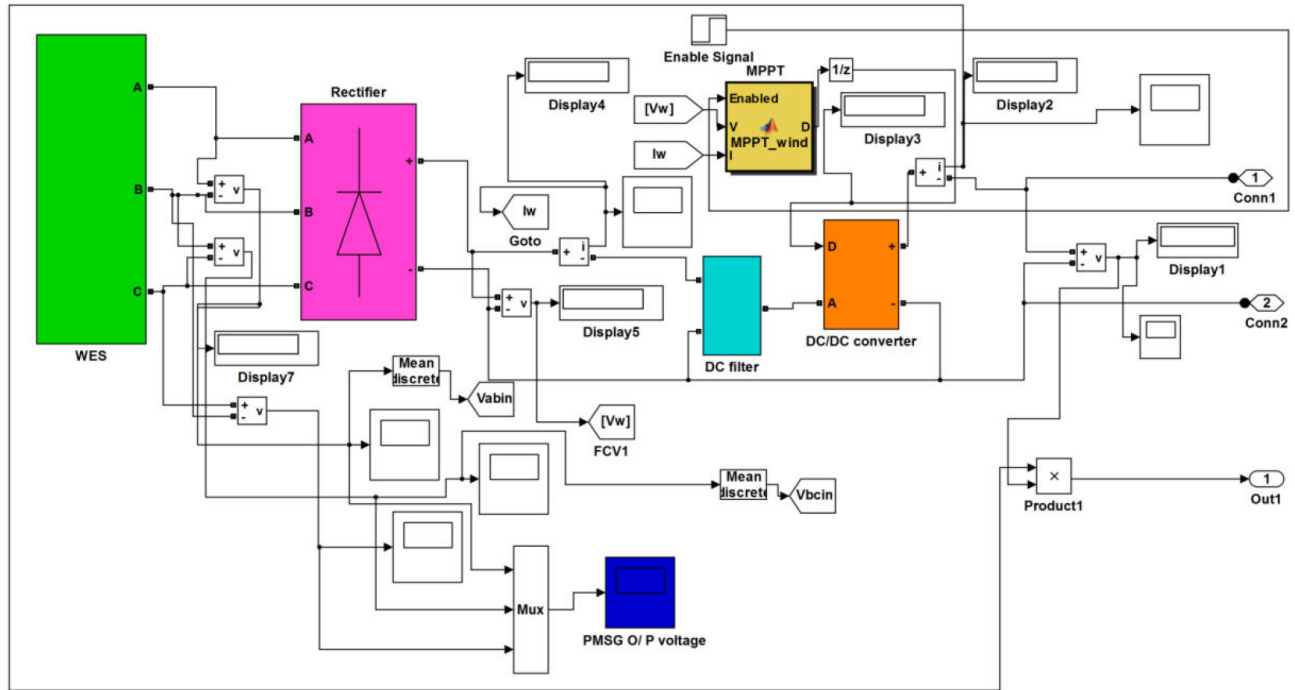**Figure 11.** MATLAB model of PMSG controller.

Figure 12. MATLAB model of WES with converter and MPPT.

5. Mathematical model of the phase-locked loop controller

The phase-locked loop (PLL) controller shown in Figure 13 is a control system that generates an output signal related to the phase of the input signal. The phase detector compares the phase of that signal with the phase of the input periodic signal and adjusts the oscillator settings such that the input and output are locked with each other. The PLL controller is used in this work where the abc parameters, in per unit values, are converted to Vdq, and this is compared in the comparator by a further process and outputs of frequency, phase, and angular speed of the turbine ω_t are obtained as controlled parameters [19].

$$3.2 * \left[\tan^{-1}\left(5 * f_m\right)\right] + \int \left[50 * \tan^{-1}\left(5 * f_m\right)\right] + n_1 = s_1 \tag{38}$$

$$S_1\left(\frac{2}{\pi}\right) = f \tag{39}$$

$$\left|\left[\left(\int s_1\right) * 2 * \pi\right]\right| = \omega t \tag{40}$$

$$f * \left[\left(\int V_q\right) - d_2\right] + C_{mp} = f_m \tag{41}$$

$$C_{mp} = V_q + \frac{1}{2}\left\{\frac{(N - N_r)}{N * (V_{q+1} - V_q) * (N - N_r)}\right\} \tag{42}$$

Here, f_m is mean frequency, f is measured frequency, N is the number of frequency samples per cycle, N_r is the round-off value of N, and n_1 is a constant.
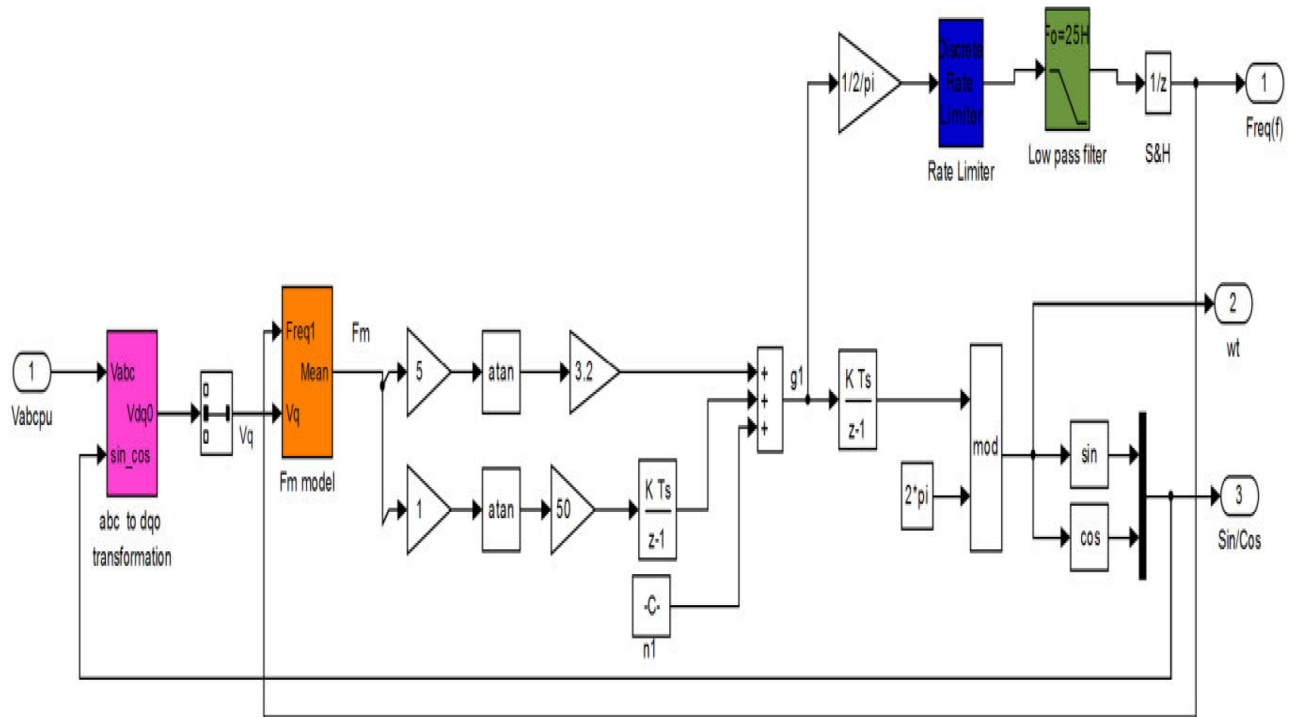
Figure 13. MATLAB model of PLL controller.

6. PV FC-WES integrated to grid

The MATLAB model of this work, i.e. the PV, FC, and WES integrated with the grid, is shown in Figure 14. The integrated setup consists of a WES with its power converters, a FC with boost converters, and a PV array with boost converters as the input renewable energy sources to act as a distributed generation setup, and the output voltage from the above sources, which is regulated in order to form a common DC bus. There are 2 DC buses in place, namely DC bus 1 and DC bus 2, where DC bus 1 is dedicated to the WES alone. The power harvested at DC bus 2 is fed to a DC filter in order to make the DC supply suitable to be fed to the 3 phase inverter. The 3 phase inverter used here is a 3 level inverter in order to eliminate the effect of the lower order harmonics, which otherwise cause distortion in the output waveform and also result in unnecessary heating.

Two AC buses are connected on either side of the 3 phase cable and a 3 phase coupling transformer. The AC bus 2 gives the input to the controller, and in the controller the parameters, namely Vabc, Iabc, and Vdc, are compared and a suitable error signal is produced and fed to the PWM generator. The PWM generator controls the inverter in such a way that the voltage and current parameters on bus 2 is always maintained at the required level.

The output of bus 2 is connected with a π-line section, which in turn connects the harvested and controlled power to the load and to the grid through bus 3. A load circuit breaker provided before the load is positioned in such a way that in the case of a heavy load and low energy production, it is possible to shed some of the unnecessary load, instead of depending on the grid. It is also possible to feed the grid with excess power generated through bus 3.
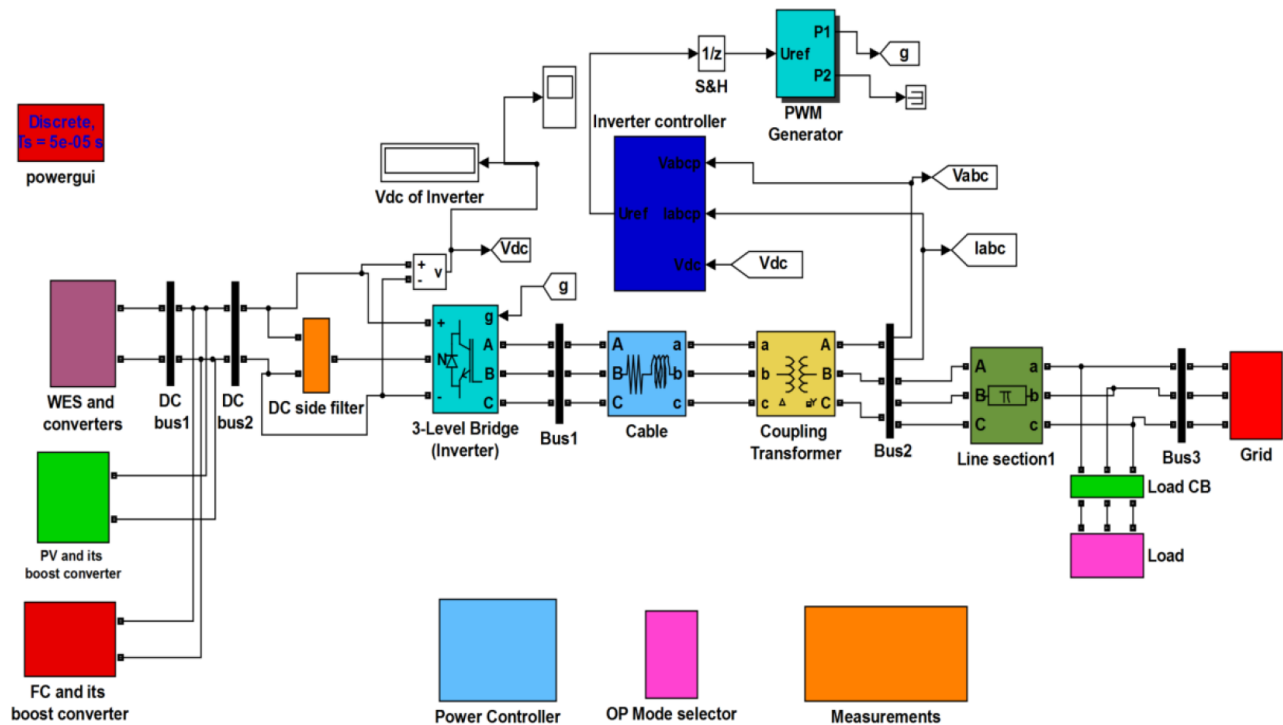
Figure 14. PV-FC-WES integrated to grid.

7. Voltage source converter controllers for power management

The VSC controller shown in Figure 15 controls the gate pulses of the 3 phase 3 level universal bridge, which is responsible for DC/AC conversion and vice versa, so that the desired power sharing between the DGs and AC grid is achieved
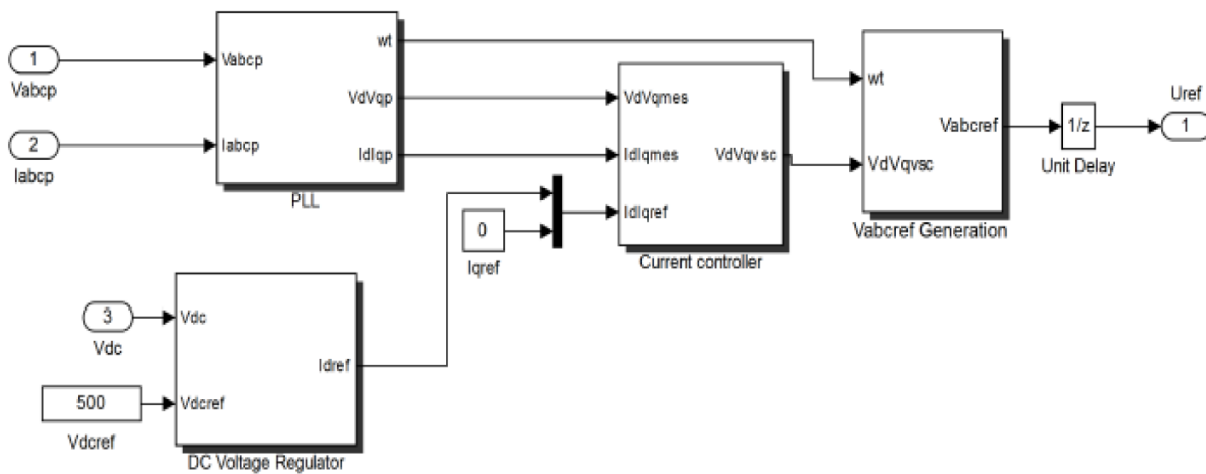

Figure 15. MATLAB model of a VSC controller.

8. Simulation results

The grid-integrated DG power system was suitably modeled and was simulated with MATLAB simulation software. The results are shown in Figure 16, which gives the output of the various renewable energy sources in the integrated DG system. In Figure 17, the first waveform corresponds to the power output of the PV system in kW. It can be seen that the output from a PV system varies with time starting with 58 kW to 78 kW, up to a maximum of 98 kW in a day.
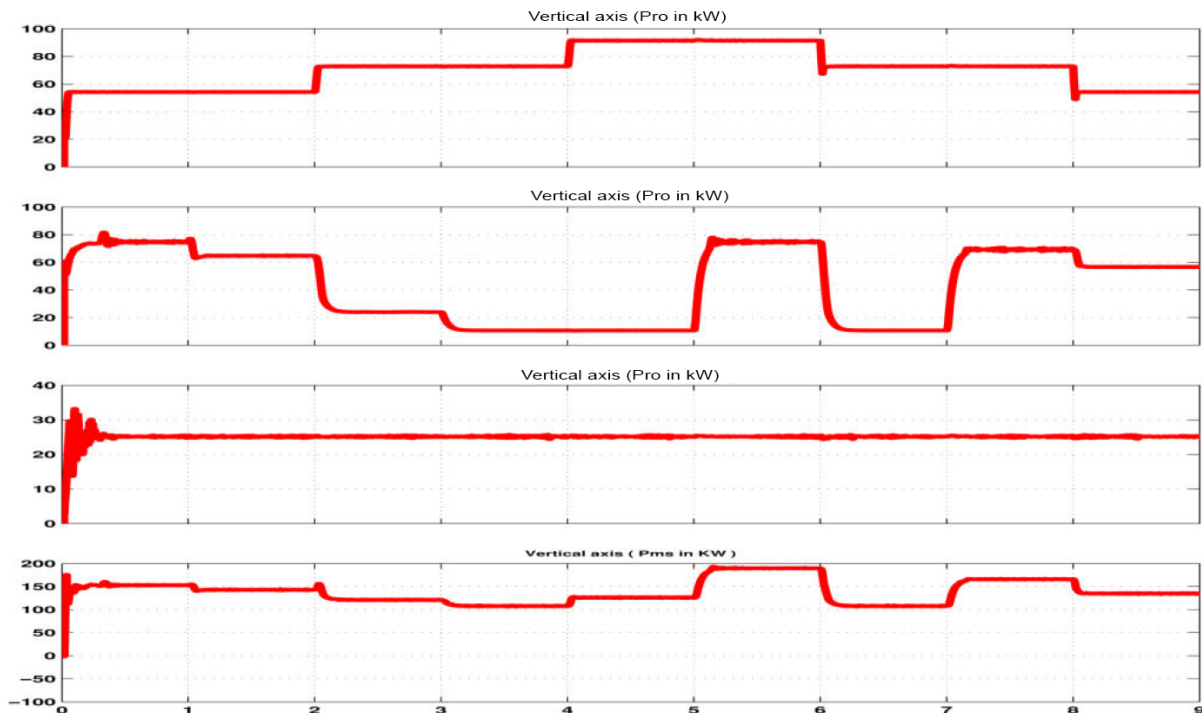
Figure 16. Output waveforms of PV, WES, and FC in kW.

The second waveform is that of the fuel cell where the reaction happening in the fuel cell makes it produce a maximum of 80 kW of power initially, which drops down to 20 kW and again to less than 80 kW. This erratic behavior is due to the fact that whenever there is an adjustment in the power requirement, the PV and WES are only controlled with the FC system being untouched. The third waveform is of the WES. With the PMSG and pitch angle control in place, the output of the WES is controlled easily in order to produce as constant of an output power as possible. The last waveform in this group is the total power available at DC bus 2 to be converted to AC. Even though there are variations in the input renewable energy, due to suitable modeling and control it can be seen that the DC bus voltage does not show a large variation in the power fed to the grid. At this point it can be seen that this system is going to feed the load with a constant power input.

The waveforms in Figure 17 show the power levels at various points of the grid-integrated system. The first waveform is the consolidated power obtained from the renewable energy sources, namely the PV arrangement, WES, and FC. The second waveform shows the load demand in kW. The third waveform shows the support provided by the grid in order to maintain the load power at a constant. Thus, whenever there is a reduction in the renewable energy output the grid is connected to compensate. In Figure 17 the last waveform shows that the voltage across the load is regulated and remains constant. This method of control is called the grid-controlled method, as stated earlier.
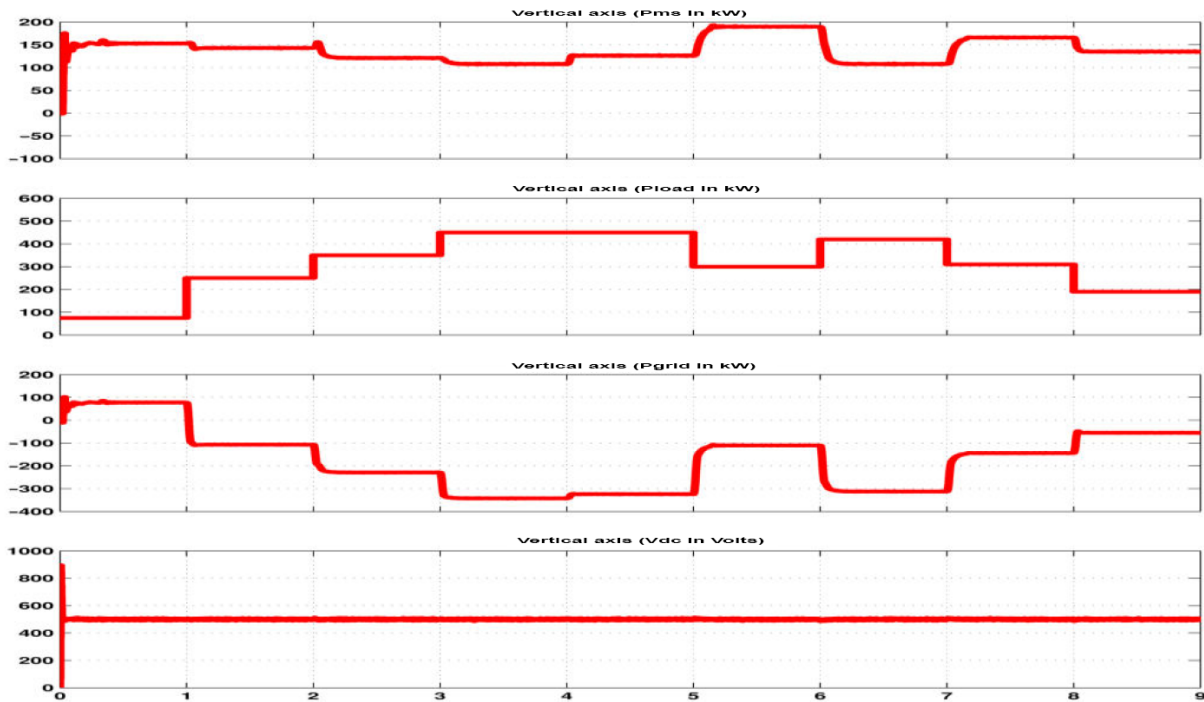
Figure 17. Waveforms depicting power flow from the sources, load, and grid.

8.1. Effect of controller on the DG output power

The effect of the control circuitry implemented in the grid-integrated distributed generation system is shown in Figure 18. It can be seen that the output of the DG system P_{ms} follows the reference P_{msref}. Thus, the controller plays an important role in maintaining the output power profile of the DG system.
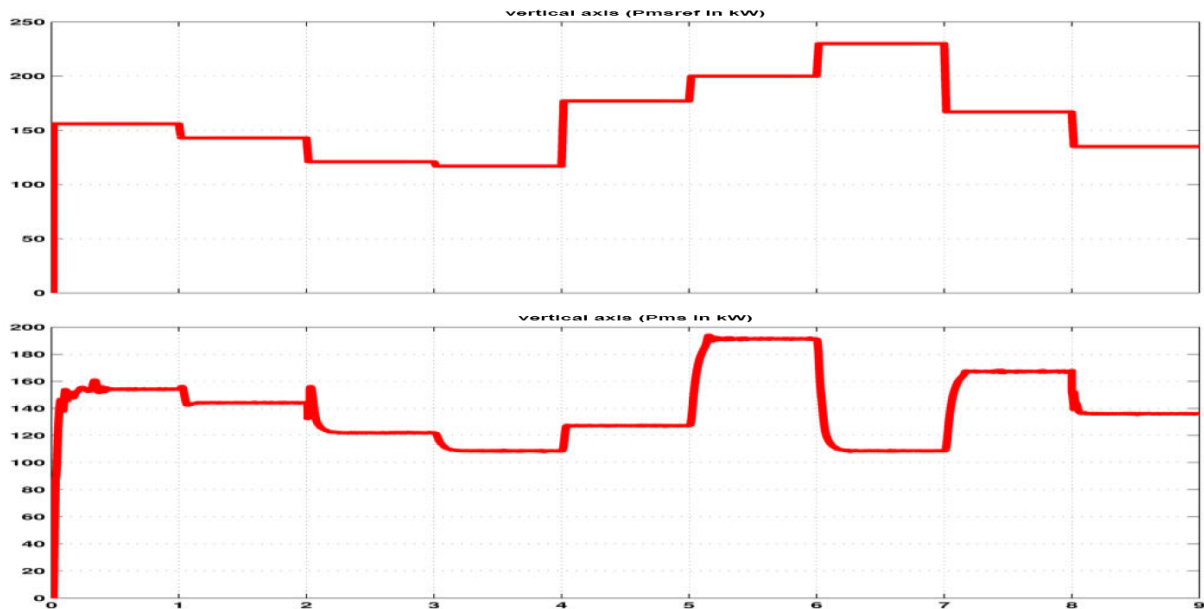

Figure 18. Effect of controller on the DG output.

In contrast, Figure 19 shows what happens when the load demand is very high. Whenever the load is high there is a feature implemented in this grid-integrated DG system in which load shedding or load curtailment is automatically applied by the controller in order to match the DG generation and to provide grid independency. For the above, the loads that are not essentially necessary when there is a dip in the DG generation are identified and curtailment is applied while other critical loads are untouched. This ensures that the grid-integrated DG system acts similar to a microgrid.
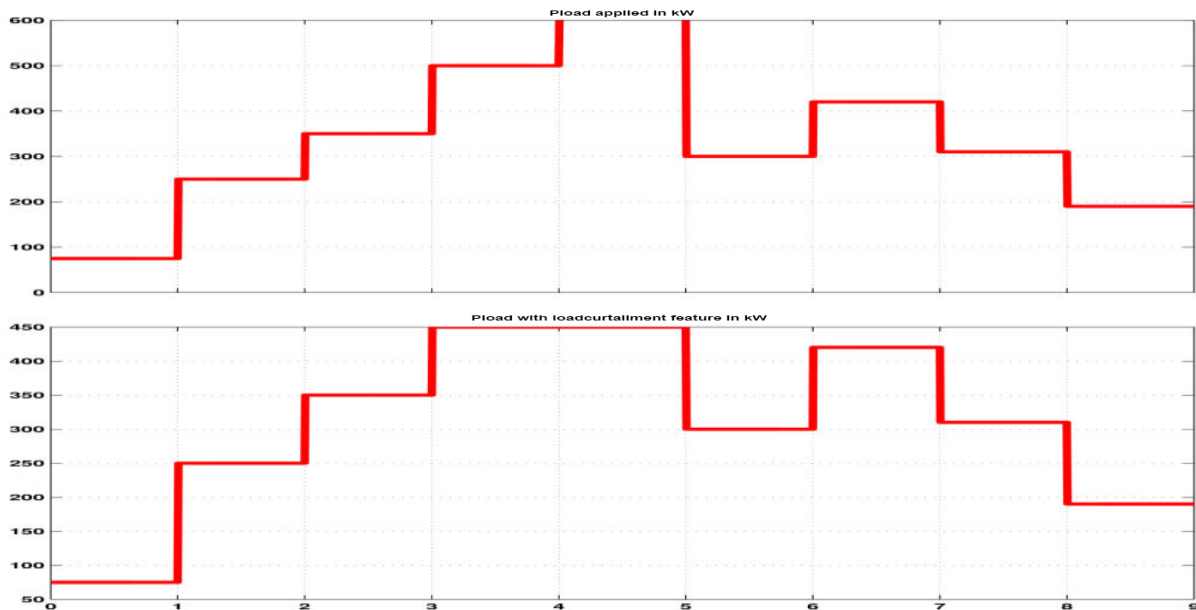
Figure 19. Waveforms depicting load curtailment feature.

9. Conclusion

From the previous sections, it can be seen that the grid-integrated hybrid DG sources of PV-FC-WES operate satisfactorily as a combination of DGCM when the load is less than the renewable power generated and in GCM when the load is greater than the renewable generation. The load shedding is implemented as and when required. The DC bus voltage is maintained constant under all load conditions, satisfying the demand and supply balance, and hence power management between DG sources, load, and grid is achieved.

The designed mathematical models and control strategies for PV, FC, WES, DC/DC converters, and inverter along with the power controller and load controller effectively achieve the smooth and satisfactory functioning of the grid-integrated hybrid system as mentioned above.

References

[1] Yang H, Wei Z, Chengzh L. Optimal design and techno economic analysis of a hybrid solar-wind power generation system. Appl Energ 2009; 86: 163-169.

[2] Mahalakshmi M, Latha S. Modeling and simulation of solar photovoltaic wind and fuel cell hybrid energy systems. Int J Eng Sci 2012; 4: 2356-2365.

[3] Wang C, Hashem NM. Power management of a stand-alone wind/photovoltaic/fuel cell energy system. IEEE T Energy Conver 2008; 23: 957-967.

[4] Khanh LN, Jae JS, Kim YS. Power management strategies for a grid connected PV-FC hybrid system. IEEE T Power Deliver 2010; 25:1874-1882.

[5] Katiraei I, Iravani MR. Power management strategies for a microgrid with multiple distributed generation units. IEEE T Power Syst 2006; 21: 1821-1831.

[6] Lu ZX, Wang CX, Min Y. Overview on microgrid research. Automation of Electric Power Systems 2007; 31: 100-107.

[7] Driesen J, Katiraei F. Design for distributed energy resources. IEEE Power Energy M 2008; 3: 30-40.

[8] Rauschenbach HS, Solar Cell Array Design Handbook. New York, NY, USA: Van Nostrand Reinhold Co., 1980.

[9] Ishaque K, Salam Z. An improved modeling method to determine the model parameters of photovoltaic modules using differential evaluation. Sol Energy 2011; 85: 2349-2359.

[10] Villalva MG, Gazoli JR, Filho ER. Comprehensive approach to modeling and simulation of photovoltaic arrays. IEEE T Power Electr 2009; 24: 1198-1208.

[11] Esram T, Chapman PL. Comparison of photovoltaic array maximum power point tracking techniques. IEEE T Energy Conver 2007; 22: 2183-2189.

[12] Noguchi T, Togashi S, Nakamoto R. Short-current pulse-based maximum-power-point tracking method for multiple photovoltaic and converter module system. IEEE T Ind Electron 2002; 49: 217-223.

[13] Jia J, Li Q, Wang Y, Cham Y T, Han M. Modelling and dynamic characteristics simulation of proton exchange membrane fuel cell. IEEE T Energy Conver 2009; 24: 2375-2381.

[14] Hajizadeh A, Golkar MA. Intelligent power management strategy of hybrid distributed generation system. Int J Elec Power 2007; 29:783-795.

[15] Leithead WE, Connor B. Control of variable speed wind turbines design task. Int J Control 2000; 13:1189-1212.

[16] Garcia Hernandez R, Garduno Ramirez R. Modeling a wind turbine synchronous generator. Int J Elec Power 2013; 2: 64-70.

[17] Ramtharan G, Jenkins N. Modelling and control of synchronous generators for wide range variable speed wind turbines. Wind Energy 2007; 10: 231-246.

[18] Chen Z, Spooner E. Grid power quality with variable speed wind turbines. IEEE T Energy Conver 2001; 16: 148-154.

[19] Kim HW, Kim SS, Ko SS. Modeling and control of PMSG based variable speed wind turbine. Electr Pow Syst Res 2010; 80: 46-52.